Field localization and enhancement of phase-locked second- and third-order harmonic generation in absorbing semiconductor cavities

V. Roppo,[1,2] C. Cojocaru,[1] F. Raineri,[3] G. D'Aguanno,[2] J. Trull,[1] Y. Halioua,[3] R. Raj,[3] I. Sagnes,[3] R. Vilaseca,[1] and M. Scalora[2]

[1]*Universitat Politècnica de Catalunya, Colom 11, E-08222 Terrassa, Spain*

[2]*Charles M. Bowden Research Facility, US Army RDECOM, Redstone Arsenal, Alabama 35803, USA*

[3]*Laboratoire de Photonique et de Nanostructures, Route de Nozay, 91460 Marcoussis, France*

(Received 4 June 2009; published 26 October 2009)

We predict and experimentally observe the enhancement by three orders of magnitude of phase mismatched second and third harmonic generation in a GaAs cavity at 650 and 433 nm, respectively, well above the absorption edge. Phase locking between the pump and the harmonics changes the effective dispersion of the medium and inhibits absorption. Despite hostile conditions the harmonics resonate inside the cavity and become amplified leading to relatively large conversion efficiencies. Field localization thus plays a pivotal role despite the presence of absorption, and ushers in a new class of semiconductor-based devices in the visible and uv ranges.

DOI: 10.1103/PhysRevA.80.043834 PACS number(s): 42.79.Nv, 42.25.Bs, 42.65.Ky, 78.67.De

Since it was discovered by Franken in the 1960s, second harmonic (SH) generation has been one of the most studied phenomena in nonlinear optics [1]. To date most efforts have been directed at improving the efficiency of the process by developing new materials with high effective nonlinear coefficients, accompanied by phase and group velocity matching [2–10]. Consequently, most studies have been concerned with maximizing conversion efficiencies, generally achievable at or very near phase matching (PM) conditions, ensuring maximum energy transfer from the fundamental beam to the harmonics. A special effort was focused toward engineering new artificial materials capable of compensating material dispersion, for example, using quasiphase matching techniques [11,12] or structured materials [13]. Outside of PM conditions, which generally coincide with low conversion efficiencies [3], the only relevant processes that have been investigated are cascaded parametric processes that can produce phase-modulation of the fundamental beam [14], pulse breaking [15] or nonlinear diffraction [16]. This has caused other possible working conditions to remain largely unexplored. A relevant feature is that in all these previous studies the nonlinear material was assumed to be transparent for both fundamental and harmonics beams, since conventional wisdom holds that an absorptive material will reabsorb any generated harmonic signal.

More recently, an effort was initiated to systematically study the behavior of SH and third harmonic (TH) fields in transparent and opaque materials under conditions of phase mismatch [17–19]. Briefly, when a pump pulse crosses an interface between a linear and a nonlinear medium there are always three generated SH (and/or TH) components. One component is generated backward into the free space, due the presence of the interface, and the remaining components are forward moving. These components may be understood on the basis of the mathematical solution of the homogeneous and inhomogeneous wave equations at the SH frequency [4]. Continuity of the tangential components of all the fields at the boundary leads to generation of the two forward-propagating components that interfere in the vicinity of the entry surface and give rise to Maker fringes [2,20] and to energy exchange between the fundamentals and SH and/or TH beams. It turns out that while the homogeneous component travels with the group velocity given by material dispersion, the inhomogeneous component is captured by the pump pulse and experiences the same effective dispersion of the pump [21]. That is, the homogenous component has wave-vector $k_{2\omega}^{HOM}=n(2\omega)k(2\omega)$ and exchanges energy with the pump until the inevitable walk off. The inhomogeneous, phase-locked (PL) component has a wave-vector $k_{2\omega}^{PL}=2n(\omega)k(\omega)$, twice the pump wave-vector, and travels locked to the pump pulse.

The consequences of phase locking can guide us toward new scenarios by allowing working conditions hitherto assumed inaccessible for absorbing materials, semiconductors in particular. In Ref. [19] it was shown that in the opaque region inhomogeneous SH and TH components are not absorbed. This behavior may be understood within the framework of the phase-locking mechanism. The real part of the effective index of refraction that the harmonics experience is equal to that of the pump [17]. This result follows from a full spectral decomposition of the wave packets in k and ω spaces, as outlined in Ref. [21]. Then, a Kramers-Kronig reconstruction of the effective index leads to a complex effective index at the harmonic wavelengths that is identical to the pump's complex index of refraction. It naturally follows that the suppression of absorption at the harmonic wavelengths will occur if the pump is tuned to a region of transparency. The only precautions to be adopted are that the pump pulses should not be too short (to avoid linear dispersion and collapse of the pump pulse), and nonlinear two-photon absorption be avoided [19]. The results reported in Refs. [19,21] are concrete evidence that phase and group velocity locking leads to the inhibition of linear absorption. The next step is to learn how to manage and exploit this ubiquitous phenomenon, possibly in spectral regions previously thought to be inaccessible.

In this paper we highlight the surprising behavior of SH and TH phase-locked components with frequencies above

the absorption edge by showing that, when the material is placed inside a cavity resonant only at the fundamental frequency, the PL mechanism not only inhibits absorption, but also fosters the enhancement of harmonic generation by several orders of magnitude compared to the no-cavity case. Our interpretation is that this enhancement arises because of two complementary factors. First, phase locking with a resonant pump (and in particular, the coincidence in the effective refractive index) pulls the harmonics into effective resonance too, leading to field localization, enhancement and increased energy exchange between the fields. In this regard, we note that the rate at which energy is transferred from a nonlinear source to a field at a harmonic frequency (for instance at frequency 2ω) is proportional to $\mathbf{J}_{2\omega}\cdot\mathbf{E}_{2\omega}$ at each point inside the material, where $\mathbf{J}_{2\omega}=\partial\mathbf{P}_{2\omega}/\partial t$ is the current density and $\mathbf{P}_{2\omega}$ is the harmonic polarization induced by the fundamental field. Since currents, polarization, and fields are local variables, the conversion efficiency depends on the strengths of both the FF and SH (or TH) fields at each point inside the cavity. Second, if the cavity filled with the nonlinear medium is short (only a few wavelengths thick), the fundamental beam inside the medium "visits" the front and rear interfaces many times during the duration of a light pulse. As shown in [17–19] and again as pointed out above, in the opaque region it is just near the surfaces that energy can flow from the pump to the harmonic fields. Far from the surfaces, once the homogenous component is absorbed, the total energy of the phase-locked component clamps and remains constant [17]. In other words, both entrance and exit interfaces are constantly traversed by the pump field and, as a result, the exiting harmonic fields are constantly generated by continuous interface crossings.

This increase in the conversion efficiency within a cavity can be illustrated with a simple numerical example, consisting of a thin layer, or free-standing etalon, of a semiconductor material, for instance GaAs, with an optical thickness of only two times the FF wavelength. This is a cavity with a relatively small Q factor. Let us assume a fundamental beam is tuned at $\lambda=1300$ nm and generates SH (650 nm) and TH (433 nm) signals. The dispersion curves for bulk GaAs [Fig. 1(a)] show that the material is transparent above $\lambda=900$ nm, and opaque below.

The complex refractive index of GaAs is $n(1300\text{ nm})=3.41$, $n(650\text{ nm})=3.83+i0.18$ and $n(433\text{ nm})=5.10+i1.35$, as reported by Palik [22]. The GaAs Fabry-Pérot etalon length (760 nm) is such that the sample is resonant at the pump wavelength, transmits ~3% of the incident light at 650 nm, and is completely opaque at 433 nm. These conditions mean that the generated SH field is dominated by the PL component, but contains some residual homogeneous signal as well and is mostly in phase with the FF field. In contrast, the TH field will contain only the phase locked component, as revealed by a k-space spectral analysis of the field eigenmodes. The thin (solid) blue curve in Fig. 1(b) shows the numerically calculated standing-wave profile of the fundamental magnetic field intensity inside the etalon. The thick (solid) red curve shows the corresponding generated SH magnetic field intensity profile. Ostensibly, the SH field pattern is in phase with that of the FF. This situation should be contrasted with the SH field generated when absorption is artificially turned off (black dashed curve). In the latter case the SH field has an odd number of peaks and does not resonate in phase with the FF due to interference between homogeneous and PL components. Although not pictured, the TH undergoes similar dynamics. Thus the PL mechanism causes the inhomogeneous components to resonate and become localized inside the cavity along with the pump, *regardless of material dispersion at the harmonic wavelengths* in what one might characterize as a double action of fundamental and *anomalous harmonic field localization*. Of course, the phenomenon occurs with any nonlinear absorbing material, including negative index materials and semiconductors in the metallic range [23]. Figure 1(b) is thus an emblematic example of anomalous field localization in media of finite thickness or cavities.

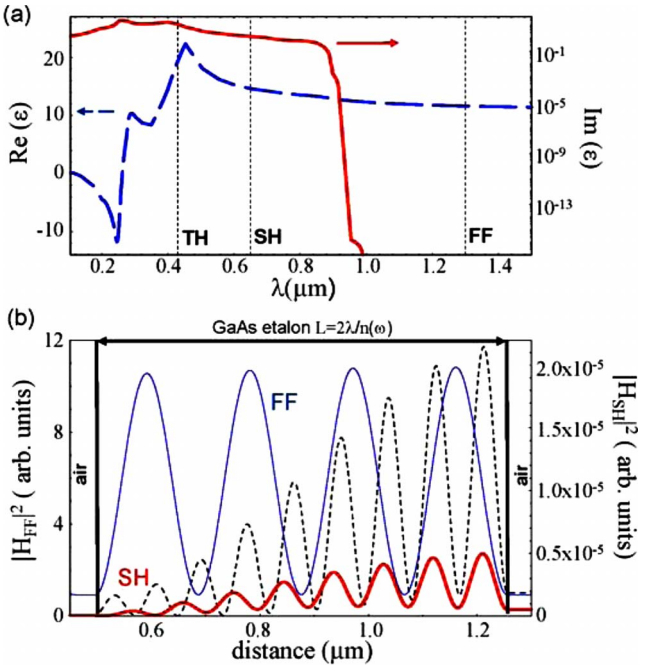

FIG. 1. (Color online) (a) Dispersion for bulk GaAs. (b) Numerical calculation of the H fields for the fundamental (FF) (thin, blue solid curve) and SH (thick, red solid curve) in an etalon two wavelengths thick. We also plot the SH field for the case where the absorption of the material is turned off (thin dashed curve). The incident field is Gaussian in shape and 80 fs in duration. It is evident that both pump and SH fields become localized (oscillations and peaks) inside the etalon, resulting in good overlap.

To model the pulsed propagation we use a numerical model similar to that used in Refs. [17–19]. The fields may be written as a superposition of harmonics as follows:

$$\mathbf{E}=\hat{\mathbf{x}}\sum_{\ell=1}^{\infty}[E_{\ell\omega}(z,t)+\text{c.c.}]=\hat{\mathbf{x}}\sum_{\ell=1}^{\infty}[\mathcal{E}_{\ell\omega}(z,t)e^{i\ell(k_0z-\omega_0t)}+\text{c.c.}],$$

$$\mathbf{H}=\hat{\mathbf{y}}\sum_{\ell=1}^{\infty}[H_{\ell\omega}(z,t)+\text{c.c.}]=\hat{\mathbf{y}}\sum_{\ell=1}^{\infty}[\mathcal{H}_{\ell\omega}(z,t)e^{i\ell(k_0z-\omega_0t)}+\text{c.c.}], \quad (1)$$

where $\mathcal{E}_{\ell\omega}(z,t),\mathcal{H}_{\ell\omega}(z,t)$ are generic, spatially, and temporally dependent, complex envelope functions; k_0 and ω_0 are

carrier wave vector and frequency, respectively, and ℓ is an integer. Equations (1) are a convenient representation of the fields, and no *a priori* assumptions are made about the field envelopes. The nonlinear polarization is assumed of the type $P_{NL}=\chi^{(2)}E^2$ where $\chi^{(2)}$ is the electric nonlinear coefficient, which may be itself be a function of position. Expanding the nonlinear polarization into its components yields the usual nonlinear polarization terms at the fundamental and second harmonic frequencies (taking only the leading terms) $\mathcal{P}_{\omega,NL}(z,t)=2\chi_{\omega}^{(2)}\mathcal{E}_{\omega}^{*}\mathcal{E}_{2\omega}$ and $\mathcal{P}_{2\omega,NL}(z,t)=\chi_{2\omega}^{(2)}\mathcal{E}_{\omega}^{2}$. Assuming that polarization and currents may be decomposed as in Eqs. (1), we obtain the following Maxwell-Lorentz system of equations for the ℓth field components, in the scaled space (ξ) and time (τ) coordinate system,

$$\frac{\partial \mathcal{E}_{\ell\omega}}{\partial \tau} = i\beta_{\ell\omega}(\mathcal{E}_{\ell\omega}-\mathcal{H}_{\ell\omega}) - 4\pi(\mathcal{J}_{\ell\omega}-i\beta_{\ell\omega}\mathcal{P}_{\ell\omega}) - \frac{\partial \mathcal{H}_{\ell\omega}}{\partial \xi} + i4\pi\beta_{\ell\omega}\mathcal{P}_{\ell\omega}^{NL} - 4\pi\frac{\partial \mathcal{P}_{\ell\omega}^{NL}}{\partial \tau},$$

$$\frac{\partial \mathcal{H}_{\ell\omega}}{\partial \tau} = i\beta_{\ell\omega}(\mathcal{H}_{\ell\omega}-\mathcal{E}_{\ell\omega}) - \frac{\partial \mathcal{E}_{\ell\omega}}{\partial \xi}, \tag{2}$$

$$\frac{\partial \mathcal{J}_{\ell\omega}}{\partial \tau} = (2i\beta_{\ell\omega}-\gamma_{\ell\omega})\mathcal{J}_{\ell\omega} + (\beta_{\ell\omega}^2 + i\gamma_{\ell\omega}\beta_{\ell\omega} - \beta_{r,\ell\omega}^2)\mathcal{P}_{\ell\omega} + \pi\omega_{p,\ell\omega}^2\mathcal{E}_{\ell\omega},$$

$$\frac{\partial \mathcal{P}_{\ell\omega}}{\partial \tau} = \mathcal{J}_{\ell\omega}.$$

In Eqs. (2), the functions $\mathcal{J}_{\ell\omega}, \mathcal{P}_{\ell\omega}, \mathcal{P}_{\ell\omega}^{NL}$ refer to linear electric currents, polarization, and nonlinear polarization, respectively. The coordinates are scaled so that $\xi=z/\lambda_0$, $\tau=ct/\lambda_0$, $\omega_0=2\pi c/\lambda_0$, where $\lambda_0=1$ μm is the reference wavelength; γ, $\beta_{\ell\omega}=2\pi\ell\omega/\omega_0$, $\beta_r=2\pi\omega_r/\omega_0$, ω_p, are the scaled damping coefficient, wave-vector, resonance, and electric plasma frequencies for the ℓth harmonic, respectively. The equations are solved using a split-step, fast Fourier transform-based pulse propagation algorithm that advances the fields in time. This method is unconditionally stable and the integrations can be carried out using criteria based on numerical convergence rather than stability tied to a relationship between temporal and spatial integration step, as is required in finite difference, time domain approaches. The envelope function representation allows for a detailed analysis of all the linear and nonlinear terms, including group velocity dispersion and self-steepening that contribute to the dynamics, without having to invoke any kind of approximation on the envelope functions, which is usually the case for the nonlinear Schrödinger equation, for example. Lastly, no undepleted pump approximation is introduced and the use of the natural space and time coordinates gives a good handle of the pulse propagation.

The conversion efficiency in the case of a simple etalon increases by several orders of magnitude with respect to the case of a bulk medium, in spite of the fact that the Q factor of the cavity is relatively small. Next, we show that slight improvements to the cavity, for example, by adding a mirror at the back interface, can lead to further improvements of conversion efficiency. By collecting both the forward and backward signals conversion efficiencies increase even more with respect to a bulk medium. We consider a GaAs layer coated with a gold mirror in the back. The calculations to optimize the GaAs cavity with the gold mirror for SH and TH emission were performed using a plane wave approach based on the Green's function for multilayered structures developed in Ref. [24]. In Fig. 2 we show the results of this theoretical study for an input intensity of ~ 5 GW/cm^2 and an incident wavelength $\lambda=1300$ nm, and compare to the SH and TH conversion efficiencies of the Fabry-Pérot etalon we discussed earlier. We assume $\chi^{(2)}\sim 14$ pm/V and $\chi^{(3)}\sim 1.7\times 10^{-19}$ m^2/V^2 in all cases. The reason for these choices will become clear later.

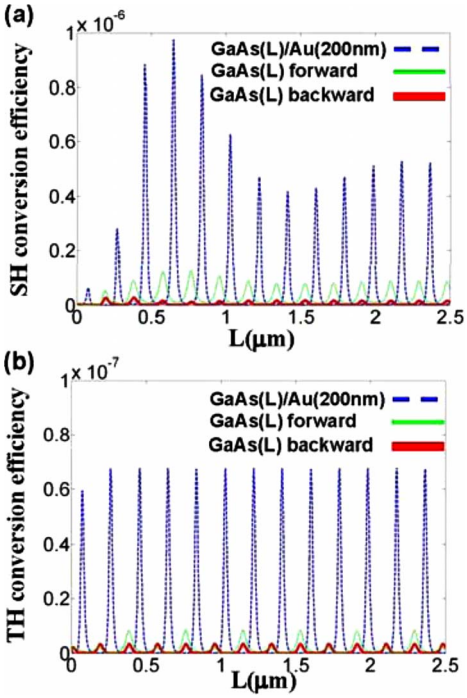

FIG. 2. (Color online) SH (a) and TH (b) conversion efficiencies vs GaAs cavity length with (dashed blue curves) and without (simple etalon, green and red curves) a back mirror. Both forward and backward harmonic generation results from the etalon.

Fig. 2(a) shows the SH conversion efficiency (dashed blue curve) as a function of cavity length, L. An absolute maximum is found for $L\sim 645$ nm, with conversion efficiency of $\sim 10^{-6}$. The peaks in the SH efficiency curve appear at the cavity lengths that make the FF field resonant. These peaks are slowly modulated by the residual presence of homogenous SH components. The TH conversion efficiency curve in Fig. 2(b) shows no such modulation, an indication that the TH signal is completely phase locked. In comparison, in Fig. 2 the thin (green) and thick (red) curves represents transmitted and reflected efficiencies, respectively, for SH [Fig. 2(a)] and TH [Fig. 2(b)] for a free-standing GaAs etalon of similar thickness. It is evident from Fig. 2 that the configuration with the back-mirror yields nonlinear conversion efficiencies one order of magnitude higher compared to a free-standing GaAs

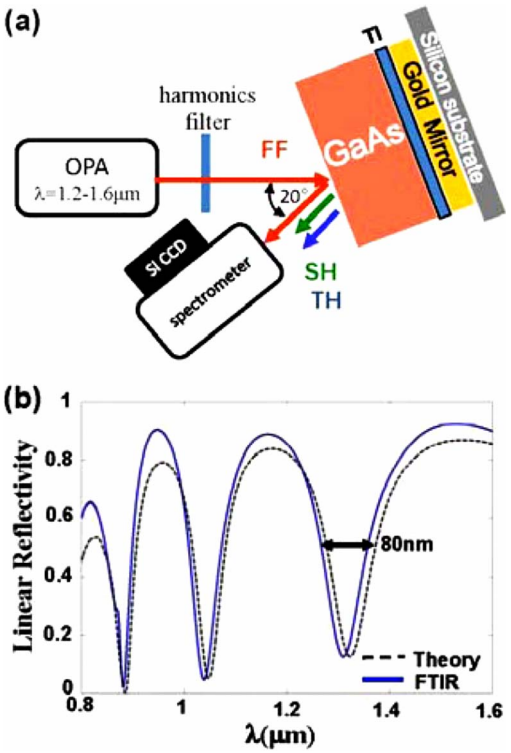

FIG. 3. (Color online) (a) Schematic of the experimental setup and the sample. (b) Linear reflectivity of the sample taken by Fourier transform infrared spectroscopy (FTIR) and comparison with theory.

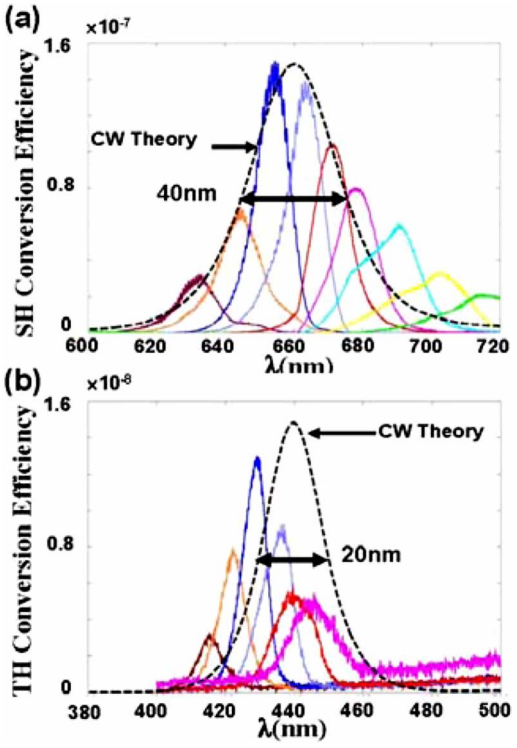

FIG. 4. (Color online) Experimental results for SH (c) and TH (d) signals. The dashed black curves represent the CW theory. The different curves represent the harmonic signals for different pump tunings (respectively from left to right 1260, 1280, 1300, 1320, 1340, 1360, 1380, 1400, 1420 nm). We note that the bandwidths of the signals are in excellent agreement with the numerical predictions.

etalon, due to enhanced field amplitudes inside the cavity. At the same time, perhaps even more remarkably, conversion efficiencies are nearly *four* orders of magnitude larger compared to the case of a GaAs bulk medium, which are of order 10^{-10} for both SH and TH for an input intensity of a few GW/cm^2 and an incidence angle of $\sim 10°$. This reference value was taken from our experiments on a SH signal generated from a GaAs substrate, and is of the same level as background noise.

We now present experimental results for a structure that we fabricated and tested in the laboratory. It corresponds to the same configuration consisting of a GaAs layer having a back gold mirror. The sample was fabricated using MOCVD to grow a 645 nm GaAs layer above a AlAs etch-stop layer, on top of a GaAs substrate. A gold mirror approximately 200 nm thick was deposited onto the GaAs layer, aided by a few nanometers of Ti buffer layer to ensure good adhesion between the metal and the semiconductor [schematization in Fig. 3(a)]. The structure was then glued upside down onto a silicon substrate using benzocyclobutene polymer [Fig. 3(a)]. Finally, the GaAs substrate and the AlAs layer were removed using mechanical grinding followed by chemical etching. The calculated and measured linear reflectances from the sample, plotted in Fig. 3(b), show that the structure displays a resonance at the FF, 1300 nm. However, the stack is not resonant at the SH and TH wavelengths. We note that the introduction of the thin Ti layer spoils cavity conditions for the pump, absorbing part of it and decreasing the total reflectance of the structure at the FF frequency from approximately 80% (without the Ti layer) down to the ~13% (with the Ti layer) shown in Fig. 3(b).

In our experiment we used a typical reflection measurement setup, shown schematically in Fig. 3(a). The source consists of (80–120) fs fundamental pulses from an OPA laser working at 1 KHz repetition rate, with tunable wavelength between 1200 and 1600 nm. The beam has a power of 200 MW and was focused on the sample down to a ~0.5 millimeter spot size, with corresponding peak intensity of ~5 GW/cm^2. The reflected signal [Fig. 3(a)] was collected and analyzed with a spectrometer connected to a cooled Si charge-coupled device (CCD) camera. The experiment consisted of scanning the sample's resonance at 1300 nm with the fundamental pulse laser, and retrieving SH and TH signals. Nine different measurements were performed from 1260 up to 1420 nm in 20 nm wavelength steps. As references, the SH and TH signals generated from a simple Au mirror and a bulk GaAs sample, as well as the background illumination, were recorded with the same setup and subtracted from the harmonic signals recorded with our sample. These references show clearly that surface SH and TH signals generated by the bulk GaAs and gold samples are negligible with respect to the harmonics generated by the cavity. The SH and TH measured for each step of the fundamental tuning are shown in Figs. 4(a) and 4(b), respectively. The vertical axis shows the conversion efficiency of each process. These results show that the maximum SH efficiency

occurs at ~650 nm and for the TH at ~435 nm: this is remarkable proof that the harmonics display resonant behavior. The dashed curve represents the envelope of the fields obtained numerically in the continuous wave (CW) regime for the cavity in our experiment, and the agreement is very good when $\chi^{(2)} \sim 14$ pm/V and $\chi^{(3)} \sim 1.7 \times 10^{-19}$ m^2/V^2. Due to field enhancement and overlap this time we recorded a SH conversion efficiency of order 1.5×10^{-7}. The presence of the Ti layer, introduced as practical solution to a mechanical gold adhesion problem, unfortunately also results in conversion efficiencies that are approximately six times smaller than what is actually possible were the Ti layer not present [Fig. 2(a)]. However, even under these conditions conversion efficiencies are at least three orders of magnitude larger than the SH signal generated by bulk GaAs under the same conditions. Even more fascinating is the TH situation, where we recorded efficiencies of order of 1.4×10^{-8} under conditions of even higher absorption and "wrong" cavity length. This is testament to the robustness of the phase-locking mechanism. Additionally to the simple illustrative examples discussed above, calculations with higher-Q cavities show that the same GaAs etalon sandwiched between distributed feedback mirrors (i.e., a photonic band gap structures with defect states) yield conversion efficiencies that rival and may even surpass conversion efficiencies from ideally phase matched layers, once again thanks to a combination of significant local field localization, enhancement, and overlap between the fundamental and harmonic fields.

As a rough estimate of what one might expect in terms of conversion efficiency Fermi's golden rule provides a good practical procedure to follow. According to this rule, the spontaneous emission rate is: $\gamma = \frac{2\pi}{\hbar} \rho(\omega) |\langle f | \boldsymbol{\mu} \cdot \mathbf{E} | i \rangle|^2$, where $|f\rangle$ and $|i\rangle$ are final and initial states, respectively, $\rho(\omega)$ is the density of states, $\boldsymbol{\mu}$ is the dipole moment, and $\mathbf{E}$ is the local electric field. Both $\rho(\omega)$ and $|\mathbf{E}|^2$ are proportional to the cavity Q. As a result nonlinear conversion rates are proportional to Q^2. One should keep in mind that these estimates are just that, and that geometrical factors like field localization, dipole position and distribution inside the cavity intervene to alter these estimates through shape factors.

The consequences of this relatively simple experiment and calculations shown here throw open new possibilities to the examination of new optical phenomena in wavelength ranges that are far below the absorption edge, well into the metallic region of semiconductors [23]. The results reported here have general validity, and apply well to semiconductors and dielectric materials alike, absorbing or not at the harmonic frequencies, as well as negative index materials, because the PL components do not experience the material dispersion characteristics at the harmonic wavelength. Finally, the right choice of materials based on the transparency window at the fundamental wavelength combined with cavity effects leads to relatively high nonlinear conversion efficiencies in GaAs at wavelengths well beyond the absorption edge, at 650 and 433 nm, respectively, with conversion efficiencies that are at least three orders of magnitude larger compared to bulk GaAs and can potentially be much higher. Our calculations show conversion efficiencies may be dramatically improved by sandwiching the GaAs etalon between distributed Bragg mirrors. This effect occurs no matter the absorption and cavity resonant conditions one finds at the SH and TH wavelengths, and it is bound to find straightforward applications, for example, in new low cost, easily tunable and easily fabricated uv and soft x-ray sources.

ACKNOWLEDGMENTS

We thank the U.S. Army European Research office for partial financial support (project W911NF). G.D. thanks the National Research Council for financial support. V.R., C.C., J.T. and R.V. acknowledge support from the Spanish government through Project No. FIS2008-06024-C03-02/FIS. We also thank Nadia Mattiucci and Mark J. Bloemer for helpful discussions and suggestions.

[1] P. A. Franken, A. E. Hill, C. W. Peters, and G. Weinreich, Phys. Rev. Lett. **7**, 118 (1961).
[2] P. D. Maker, R. W. Terhune, M. Nisenhoff, and C. M. Savage, Phys. Rev. Lett. **8**, 21 (1962).
[3] J. A. Armstrong, N. Bloembergen, J. Ducuing, and P. S. Pershan, Phys. Rev. **127**, 1918 (1962).
[4] N. Bloembergen and P. S. Pershan, Phys. Rev. **128**, 606 (1962).
[5] S. L. Shapiro, Appl. Phys. Lett. **13**, 19 (1968).
[6] W. H. Glenn, IEEE J. Quantum Electron. **5**, 284 (1969).
[7] J. T. Manassah and O. R. Cockings, Opt. Lett. **12**, 1005 (1987).
[8] L. D. Noordam, H. J. Bakker, M. P. de Boer, and H. B. van Linden van den Heuvell, Opt. Lett. **15**, 1464 (1990).
[9] R. M. Rassoul, A. Ivanov, E. Freysz, A. Ducasse, and F. Hache, Opt. Lett. **22**, 268 (1997).
[10] W. Su, L. Qian, H. Luo, X. Fu, H. Zhu, T. Wang, K. Beckwitt, Y. Chen, and F. Wise, J. Opt. Soc. Am. B **23**, 51 (2006).
[11] A. Feisst and P. Koidl, Appl. Phys. Lett. **47**, 1125 (1985).
[12] G. A. Magel, M. M. Fejer, and R. L. Byer, Appl. Phys. Lett. **56**, 108 (1990).
[13] J. P. van der Ziel and M. Ilegems, Appl. Phys. Lett. **28**, 437 (1976); K. Sakoda and K. Othaka, Phys. Rev. B **54**, 5742 (1996); Y. Dumeige, P. Vidakovic, S. Sauvage, I. Sagnes, J. A. Levenson, C. Sibilia, M. Centini, G. D'Aguanno, and M. Scalora, Appl. Phys. Lett. **78**, 3021 (2001).
[14] R. J. De Salvo, D. J. Hagan, M. Sheik-Bahae, G. Stegeman, E. W. Van Stryland, and H. Vanherzeele, Opt. Lett. **17**, 28 (1992).
[15] E. Fazio, M. Zitelli, S. Dominici, C. Sibilia, G. D'Aguanno, and M. Bertolotti, Opt. Commun. **148**, 427 (1998).
[16] S. Saltiel, D. N. Neshev, W. Krolikowski, A. Arie, O. Bang, and Y. S. Kivshar, Opt. Lett. **34**, 848 (2009).
[17] V. Roppo, M. Centini, C. Sibilia, M. Bertolotti, D. de Ceglia, M. Scalora, N. Akozbek, M. J. Bloemer, J. W. Haus, O. G. Kosareva, and V. P. Kandidov, Phys. Rev. A **76**, 033829 (2007).

[18] V. Roppo, M. Centini, D. de Ceglia, M. A. Vicenti, J. W. Haus, N. Akozbek, M. J. Bloemer, and M. Scalora, Metamaterials **2**, 135 (2008).
[19] M. Centini, V. Roppo, E. Fazio, F. Pettazzi, C. Sibilia, J. W. Haus, J. V. Foreman, N. Akozbek, M. J. Bloemer, and M. Scalora, Phys. Rev. Lett. **101**, 113905 (2008).
[20] J. Jerphagnon and S. K. Kurtz, J. Appl. Phys. **41**, 1667 (1970).
[21] E. Fazio, F. Pettazzi, M. Centini, M. Chauvet, A. Belardini, M. Alonzo, C. Sibilia, M. Bertolotti, and M. Scalora, Opt. Express **17**, 3141 (2009).
[22] E. D. Palik, *Handbook of Optical Constants of Solids* (Academic Press, New York, 1985).
[23] N. Akozbek *et al.*, e-print arXiv:0904.4082v1.
[24] N. Mattiucci, G. D'Aguanno, M. J. Bloemer, and M. Scalora, Phys. Rev. E **72**, 066612 (2005).